Mutagenesis of p38α MAP Kinase Establishes Key Roles of Phe169 in Function and Structural Dynamics and Reveals a Novel DFG-OUT State

Marina Bukhtiyarova, Michael Karpusas, Katrina Northrop, Haridasan V. M. Namboodiri, and Eric B. Springman*

Department of Biology, Locus Pharmaceuticals, Inc., Four Valley Square, 512 Township Line Road, Blue Bell, Pennsylvania 19422

Received October 25, 2006; Revised Manuscript Received March 5, 2007

ABSTRACT: In order to study the role of Phe169 in p38α MAP kinase structure and function, wild-type p38α and five p38α DFG motif mutants were examined *in vitro* for phosphorylation by MKK6, kinase activity toward ATF2 substrate, thermal stability, and X-ray crystal structure. All six p38α variants were efficiently phosphorylated by MKK6. However, only one activated p38α mutant (F169Y) possessed measurable kinase activity (1% compared to wild-type). The loss of kinase activity among the DFG mutants may result from an inability to correctly position Asp168 in the activated form of p38α. Two mutations significantly increased the thermal stability of p38α (F169A $\Delta T_m = 1.3$ °C and D168G $\Delta T_m = 3.8$ °C), and two mutations significantly decreased the stability of p38α (F169R $\Delta T_m = -3.2$ °C and F169G $\Delta T_m = -4.7$ °C). Interestingly, X-ray crystal structures of two thermally destabilized p38α-F169R and p38α-F169G mutants revealed a DFG-OUT conformation in the absence of an inhibitor molecule. This DFG-OUT conformation, termed α-DFG-OUT, is different from the ones previously identified in p38α crystal structures with bound inhibitors and postulated from high-temperature molecular dynamics simulations. Taken together, these results indicate that Phe169 is optimized for p38α functional activity and structural dynamics, rather than for structural stability. The α-DFG-OUT conformation observed for p38α-F169R and p38α-F169G may represent a naturally occurring intermediate state of p38α that provides access for binding of allosteric inhibitors. A model of the local forces driving the DFG IN−OUT transition in p38α is proposed.

p38α mitogen-activated protein (MAP) kinase[1] (E.C. 2.7.1.37) is a serine-threonine protein kinase that plays a central role in the regulation of proinflammatory stress-response pathways. In the absence of stress-response signaling, the intracellular pool of p38α protein exists in a largely unphosphorylated and catalytically inactive state. Upon activation of stress signaling pathways, upstream kinases including MKK3 and MKK6 activate p38α by phosphorylation of Thr180 and Tyr182, which are located in the p38α activation loop in close proximity to the ATP and substrate binding sites (*1*, *2*). Once activated, p38α subsequently phosphorylates and activates an array of downstream substrates including other protein kinases (MAPKAP kinase-2/3, MNK1, MSK, and PRAK) and transcriptional factors (ATF-2, MEF2C, and Elk-1). p38α signaling ultimately results in significant transcriptional and translational up-regulation of several proinflammatory cytokines including tumor necrosis factor alpha (TNFα), interleukin-1beta (IL-1β), interleukin-6 (IL-6), and interleukin-8 (IL-8), as well as the proinflammatory prostaglandin pathway via cyclooxygenase-2 (COX-2) (*3*, *4*). Because of its prominent role as an activator of inflammatory responses, p38α has been the subject of extensive research toward development of small molecule inhibitor drugs for the treatment of inflammatory and autoimmune diseases, including rheumatoid arthritis, inflammatory bowel disease, and osteoporosis.

A widely conserved feature among protein kinase superfamily members is a stretch of three amino acids in the activation loop called the DFG motif, which is composed of Asp168, Phe169, and Gly170 in p38α (*5*, *6*, *7*). The aspartic acid residue in the DFG motif (Asp168 in p38α) is important for catalysis because it is responsible for coordinating a magnesium ion that aids in the positioning of the gamma phosphate of ATP for hydrolysis (*5*). Thus, positioning of the DFG loop aspartic acid is thought to be critical for the ATP hydrolytic activity of p38α and other protein kinases.

A picture of the dynamic nature of the DFG loop in p38α is rapidly emerging. The DFG motif is known to behave as a structurally dynamic element in some protein kinases, such as Src and Abl where conformational changes in the DFG motif play a role in regulating enzyme activity (*8*). In p38α, the DFG loop has been shown to be structurally dynamic in response to the binding of a class of diarylurea inhibitors (*9*, *10*). These inhibitors bind, in part, to a cavity that is only accessible as a result of a large conformational change in the DFG motif (called DFG-OUT). This type of inhibitor binding, sometimes called allosteric inhibitor binding, has now been observed in many protein kinases (*11*, *12*, *13*). The DFG-OUT conformation and a pseudo-DFG-OUT conformation were observed for p38α in the absence of an

* Corresponding author. E-mail: espringman@locuspharma.com. Phone: 215-358-2009. Fax: 215-358-2030.

[1] Abbreviations: MAP kinase, mitogen activated protein kinase; MKK6, mitogen activated protein kinase kinase 6; GST-ATF2, fusion protein of gluthione-S-transferase and activating transcription factor 2; DTT, dithiothreitol; SDS−PAGE, sodium dodecylsulfate polyacrylamide gel electrophoresis; DFG, Asp168-Phe169-Gly170 in p38α.

10.1021/bi0622221 CCC: $37.00
Published on Web 04/19/2007

inhibitor during high-temperature molecular dynamics simulations, and NMR evidence supported the existence of a dynamic equilibrium between DFG-IN and DFG-OUT conformations of apo-p38α (*14*, *15*). A recently reported cocrystal structure of p38α with SB-203580, an ATP-site inhibitor which was previously only known to bind to p38α in the DFG-IN conformation, showed that SB-203580 could bind to the ATP-binding site of p38α in either the DFG-IN or DFG-OUT conformation (*15*). To date, the structure of the DFG-OUT conformation of p38α has only been empirically determined in the presence of a bound inhibitor.

Here, the role of Phe169 in p38α has been studied with respect to activation, catalytic activity, thermal stability, and structure by creating a probe set of p38α proteins containing mutations in the DFG loop. Our findings suggest that Phe169 in the p38α DFG loop is optimized for catalytic activity rather than for structural stability and that the p38α DFG loop is likely to be structurally dynamic in the absence of inhibitor binding. A novel DFG-OUT conformation has been discovered in unliganded p38α, and this conformation could represent the naturally occurring intermediate state that provides access to the Phe169 cavity for allosteric inhibitor binding. This new experimentally observed DFG-OUT conformation is termed α-DFG-OUT to reflect the alpha-helix-like conformation adopted by Asp168, which contrasts with the beta-sheet-like conformation of Asp168 observed in the inhibitor bound structures described in PDB entries 1KV1 and 2EWA (*9*, *15*). Based on these results and observations, a model is presented for the local forces driving DFG loop dynamics in p38α in the absence of inhibitor binding.

MATERIALS AND METHODS

Site-Directed Mutagenesis. A plasmid containing the murine p38α full-length amino acid sequence with a His-tag of seven amino acid residues at the amino terminus was used as a template for mutagenesis (*16*). Oligonucleotides for PCR and DNA sequencing were purchased from Invitrogen (Carlsbad, CA). PCR reagents, restriction and DNA modifying enzymes were obtained from New England Biolabs (Beverly, MA), Invitrogen, or Promega (Madison, WI). Plasmid DNA samples were isolated using the Qiagen (Valencia, CA) DNA mini-prep. Mutagenesis was performed using the Stratagene (La Jolla, CA) QuikChange Site-Directed Mutagenesis Kit according to the manufacturer's protocol. Synthetic nucleotide primers in conjunction with their reverse complements (each 40 bases long) were used to generate p38α-F169R, p38α-F169G, p38α-F169Y, and p38α-F169A. The following sequence was used for the forward primer: 5′-GAGCTCAAGATTCTGGATTTTGGG-CTGGCTCGGCACACTG-3′, where the Phe169 mutation site is underlined. The mutagenesis oligonucleotides contained the following changes to the phenylalanine codon locus: p38α-F169R, TTT → CGT; p38α-F169G, TTT → GGC; p38α-F169Y, TTT → TAT, and p38α-F169A, TTT → GCC. To generate p38α-D168G, a 33-base oligonucleotide was used with the following sequence for the forward primer (the mutation site is underlined) 5′-CTCAAGATTCTG-GGTTTTGGGCTGGCTCGGCAC-3′. For each p38α mutant, the entire coding region was subjected to DNA sequence analysis to verify the correct sequence.

Protein Expression and Purification. Wild-type and mutant forms of p38α protein were expressed in *Escherichia coli* as described previously (*16*). For each protein variant, a culture of *E. coli* Rosetta DE3 cells (Novagen, Madison, WI) harboring the expression plasmid was grown in 1 L of standard Luria−Bertani (LB) broth containing 100 μg/mL ampicillin. The cultures were incubated at 37 °C until A_{600} reached 0.5, and then the flasks were transferred to 30 °C. After 30 min at 30 °C, expression of p38α protein was induced by addition of 1 mM isopropyl-1-thio-β-D-galactopyranoside (IPTG) (Sigma, St. Louis, MO). Cells were harvested after another 3 h growth in the presence of IPTG at 30 °C. Cell pellets were either immediately used or stored frozen at −20 °C.

For protein purification, the bacterial cell pellet was resuspended in a lysis buffer containing 50 mM Tris, pH 7.4, 500 mM NaCl, and 10 mM imidazole. Cell lysis was performed using an EmulsiFlex-C5 homogenizer (Avestin, Canada). After centrifugation, the supernatant was applied to a Metal Chelate Ni^{2+} XK 16/20 column (GE Healthcare, Piscataway, NJ), previously equilibrated with the lysis buffer. Protein was eluted with an imidazole gradient. The p38α-containing fractions were combined and dialyzed overnight at 4 °C against 50 mM Tris, pH 7.4, 100 mM NaCl, 1 mM DTT buffer. p38α was further purified by chromatography on Mono Q HR 10/10 column (GE Healthcare, Piscataway, NJ) equilibrated in 50 mM Tris, pH 7.4, 50 mM NaCl, 5% glycerol, 10 mM $MgCl_2$, and 1 mM DTT. Protein was eluted with a linear NaCl gradient. Protein concentrations were determined by the Micro BCA Protein Assay Reagent Kit with bovine serum albumin as a standard (Pierce Biotechnology, Rockford, IL) using a Cary 100 Bio UV visible spectrophotometer (Varian Analytical Instruments, Walnut Creek, CA). The protein purity of all p38α variants was greater than 95% as assessed by Coomassie staining of SDS−PAGE gels. The purified proteins were concentrated to 16−28 mg/mL, divided into aliquots, flash frozen in liquid nitrogen, and stored at −80 C°. Typically, from 50 to 80 mg of p38α protein was produced from 1 L of bacterial cell culture after purification.

Thermal Denaturation. Thermal denaturation experiments were carried out by monitoring the intrinsic fluorescence of unphosphorylated wild-type p38α and each DFG mutant at an excitation wavelength of 280 nm and an emission wavelength of 340 nm using a Cary Eclipse fluorescence spectrophotometer (Varian Analytical Instruments, Walnut Creek, CA). Samples for thermal denaturation analysis contained 1.8 μM p38α protein in 25 mM Tris, pH 7.5, 100 mM sodium chloride, 10 mM $MgCl_2$, 5% glycerol, and 10 mM DTT buffer. Prior to analysis, the protein samples were transferred into cuvettes and allowed to equilibrate for 10 min at room temperature. The individual cuvettes were securely capped to prevent evaporation and stationed in a thermostatically controlled cuvette holder. Temperature-dependent analyses were conducted by steadily increasing the cuvette temperature at a rate of 1 °C/min from 20 °C to 80 °C, while continuously monitoring fluorescence. Ten independent experiments were performed for wild-type p38α, and two independent experiments were performed for each p38α mutant to accurately resolve the thermal stability. For control samples, containing buffer in the absence of p38α protein, there was no significant fluorescence signal detected

over the temperature range tested. Thermal denaturation of p38α was observed as a rapid increase in fluorescence over a narrow temperature range. Thermal denaturation data was processed in a manner similar to methods previously described (*17*, *18*). Briefly, the fluorescence signal was normalized and converted to fraction of unfolded p38α as a function of temperature. First, a linear baseline was determined for the fluorescence signal over a range of temperatures immediately preceding and following the p38α melting transition range. The linear baseline was subtracted from the raw fluorescence signal in order to account for changes in fluorescence over temperature not related to changes in p38α folding state. The baseline-corrected data was then normalized based on the premise that prior to the melting transition no p38α is unfolded and subsequent to the melting transition all p38α is unfolded. Accordingly, each baseline-corrected data point was divided by the extrapolated maximum fluorescence signal representing the completely unfolded state, yielding a minimum of 0 and a normalized maximum of 1. To determine the thermal melting temperature (T_m), the resulting thermal melting curves were fit to the following Boltzmann sigmoidal equation assuming no change in heat capacity over the temperature range: fraction unfolded = $1/(1 + \exp((T_m - T)/\text{slope}))$. For wild-type p38α, the standard deviation of T_m averaged less than 0.24 °C over 10 experiments using this method.

Phosphorylation of p38α Variants by MKK6. Purified p38α wild-type and mutant proteins were phosphorylated *in vitro* by treatment with the protein kinase MKK6 (Sigma, St. Louis, MO). Phosphorylation reactions were carried out in a final volume of 100 μL of 25 mM HEPES buffer, pH 7.4, containing 10 mM $MgCl_2$ and 2 mM DTT. Non-phosphorylated proteins (1 μM) were incubated with 10 nM MKK6 and 1 mM ATP for 90 min at 30 °C; then samples were diluted to suitable working concentrations and used in enzyme activity studies. The extent of p38α phosphorylation was examined by Western blot analysis using a monoclonal phospho-p38α MAP kinase Thr180/Tyr182 antibody that specifically recognizes p38α protein that is dually phosphorylated at residues Thr180 and Tyr182 (Cell Signaling Technology, Danvers, MA).

Protein samples were normalized for the amount of protein loaded on the gel to allow semiquantitative comparison of p38α samples and resolved by SDS−PAGE. Proteins were stained with Coomassie or transferred to a nitrocellulose membrane (Invitrogen, Carlsbad, CA), and probed with phospho-specific antibody to visualize bis-phosphorylated p38α protein. Immune complexes were detected using Renaissance Western Blot Chemiluminescence Reagent, NEN Life Science Products (Boston, MA), according to the manufacturer's recommendations.

Protein Kinase Activity Assay. The enzymatic protein kinase activity of each dually phosphorylated p38α protein variant was determined by measuring the incorporation of ^{33}P from γ-[^{33}P]ATP into the GST-ATF2 substrate, amino acids 19−96 (Upstate, Charlottesville, VA). Wild-type p38α was tested at 2 nM enzyme in the assay and the p38α mutants were tested at 10 nM enzyme to discern low activity levels. Substrate phosphorylation reactions were carried out in a final volume of 50 μL of 24 mM Tris-HCl buffer, pH 7.5, containing 13 mM $MgCl_2$, 12% glycerol, 2% DMSO, 2 mM DTT, 2.5 μCi of [γ-^{33}P]ATP (1000 Ci/mmol; 1 Ci = 37 GBq) (GE Healthcare, Piscataway, NJ), 10 μM cold ATP (GE Healthcare, Piscataway, NJ), and 2 μM GST-ATF2 substrate. The assays were initiated by simultaneous addition of GST-ATF2 and ATP. Reaction mixtures were incubated for 70 min at 30 °C before being stopped by the addition of 10 μL of 600 mM phosphoric acid. Phosphorylated protein substrate was captured on a phosphocellulose 96-well plate (Millipore MAPHNOB 10), washed with 100 mM phosphoric acid, and counted in a BeckmanCoulter LS6500 liquid scintillation counter.

Determination of Crystal Structures. Crystallization of each p38α mutant was carried out as previously described for wild-type p38α (*16*). Briefly, a concentrated solution of each p38α protein variant (approximately 16 mg/mL) was mixed with reservoir solution (10−20% PEG 4000, 0.1 M cacodylic acid pH 6, 50 mM *n*-octyl-β-D-glucoside) at a 3:2 protein/solution volume ratio. Hanging or sitting drops of the mixture were placed over the reservoir solution, and crystals were grown by vapor diffusion at 20 °C. Seeding with a dilute solution of crushed crystals was often used to accelerate nucleation. The resulting crystals were rod shaped, were relatively easy to reproduce, and reached a maximum size of 0.3 × 0.3 × 1 mm within 24−72 h. The best quality diffraction data was obtained using crystals that were not more than 7 days old. For cryoprotection, crystals were gradually transferred to a solution of 18% ethylene glycol, 25% PEG 4000, 0.1 M cacodylic acid pH 6 and were flash-frozen in liquid nitrogen.

X-ray diffraction data were collected at 100 K, using an ADSC Quantum 4 CCD detector at the X4A beamline of the National Synchrotron Light Source, Brookhaven National Laboratory (Upton, NY). The data were processed with the HKL program package (*19*). Analysis of diffraction data using the HKL programs indicated that the crystals were orthorhombic, of space group $P2_12_12_1$ and approximate cell dimensions 67.7, 70.5, 76.3 Å. Molecular replacement and crystallographic refinement were performed using the CNX program package (*20*) (Accelrys, Inc.), and molecular graphics manipulations were done with the program QUANTA (Accelrys, Inc.). X-ray diffraction data showed that crystals diffracted to 2.0−2.3 Å resolution. Additional crystallographic parameters are supplied as Supporting Information. Atomic coordinates are being deposited in the RCSB Protein Data Bank.

RESULTS

Expression and Purification. Phe169 is conserved among p38 isotypes and also broadly among protein kinases (*7*). This amino acid is located adjacent to Asp168, which is highly conserved and required for ATP hydrolysis (*5*, *21*). Asp168 also constitutes the first residue of the now well-known DFG motif, which is a structurally dynamic feature of the p38α activation loop (*9*, *22*). In order to investigate the functional and structural roles of Phe169 in p38α MAP kinase, we employed site-directed mutagenesis to generate five mutants: p38α-F169R, p38α-F169G, p38α-F169Y, p38α-F169A, and p38α-D168G. In p38α-F169A the phenyl group of the Phe169 side chain is removed, leaving only the methyl group of the Ala169 beta carbon as a small and aliphatic side chain. In p38α-F169Y the aromatic ring is conserved but a hydroxyl group is introduced in the para

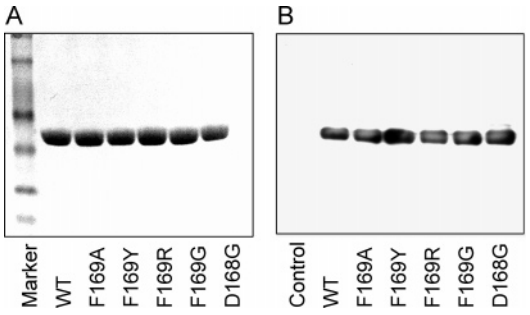

FIGURE 1: Purified wild-type p38α and DFG mutants and *in vitro* phosphorylation by MKK6. Purified p38α wild-type and DFG mutants (panel A) were phosphorylated *in vitro* by active MKK6 kinase (panel B). Panel A: 5 μg of each MKK6-treated p38α sample was loaded on a SDS−PAGE gel and stained with Coomassie. Panel B: 5 ng of each MKK6-treated p38α sample was loaded on a SDS−PAGE gel, transferred to a nitrocellulose membrane, and probed with phospho-p38α Thr180/Tyr182 specific antibody to visualize double phosphorylated p38α protein. Control is untreated p38α wild-type.

position of the phenyl group, making the side chain slightly larger and more polar. In p38α-F169R the side chain is long and positively charged. In p38α-F169G, the side chain is completely removed and the backbone is more flexible. p38α-D168G was created to test the effect of additional flexibility in the DFG motif. In this case the Asp168 side chain, which is responsible for coordination of Mg^{2+} and positioning of the ATP gamma phosphate, is lost and the mutant is not expected to retain catalytic activity. All p38α variants were overexpressed in *E. coli* as amino-terminal His-tagged proteins and purified using an efficient two-step protocol (*16*). Overall, the DFG mutants behaved similarly to the wild-type p38α protein during expression and purification. Each p38α variant was obtained in milligram per liter quantities and purified to more than 95% homogeneity as assessed by SDS−PAGE and Coomassie staining (Figure 1A).

Functional Characterization. To characterize the biochemical properties of the purified DFG mutants, *in vitro* phosphorylation of the p38α variants by MKK6 kinase was carried out, and the ability of the phosphorylated p38α variants to phosphorylate GST-ATF2 was tested. Prior to treatment with MKK6, the wild-type and DFG mutant p38α proteins expressed in *E. coli* showed no detectable levels of autophosphorylation and did not display any intrinsic ability to phosphorylate GST-ATF2 (data not shown).

Recombinant wild-type and DFG mutant p38α proteins were treated with MKK6 (a natural activator of p38α) in the presence of ATP. The extent of p38α phosphorylation was examined by Western blot analysis using a phospho-Thr180/Tyr182-p38α MAP kinase antibody, which detects p38α MAP kinase only when dually phosphorylated at Thr180 and Tyr182. Non-phosphorylated wild-type p38α was included as a negative control for Western blot analysis. The results presented in Figure 1B show that wild-type p38α and all five DFG mutants were efficiently phosphorylated *in vitro* with a comparable level of dual phosphorylation.

Dually phosphorylated (activated) wild-type and DFG mutant p38α proteins were tested in an *in vitro* kinase assay using GST-ATF2 as the protein substrate in the presence of ATP. This assay indicated that even though all five DFG mutants were fully phosphorylated, their enzymatic activity was dramatically reduced compared to wild-type p38α. As expected, removal of the catalytic aspartate side chain in p38α-D168G resulted in a catalytically inactive protein. Of the four Phe169 mutants, only p38α-F169Y exhibited measurable protein kinase activity (1%) compared to wild-type p38α treated and tested in the same manner (Table 1).

Table 1: Comparison of Structural and Functional Properties of p38α Wild-Type and Mutant Forms

p38α form	T_m °C	ΔT_m^{wt} °C	DFG IN	DFG OUT	D168 φ deg	D168 ψ deg	phospho[a] %	act.[b] %
D168G	54.5	3.8	yes	weak	118[c]	2[c]	100	<1
F169A	52.0	1.3	yes	no	59	28	100	<1
WT[e]	50.7		yes	no	44	52	100	100
F169Y	50.6	−0.1	yes	weak	56[c]	45[c]	100	1
F169G	47.5	−3.2	no	yes	−82	−22	100	<1
F169R	46.0	−4.7	weak	yes	−69[d]	−35[d]	100	<1

[a] Phosphorylation of p38α Thr180 and Tyr182 by MKK6, relative to WT. [b] Phosphorylation of GST-ATF2 by activated p38α, relative to WT. [c] DFG-IN conformation. [d] DFG-OUT conformation. [e] Structural data from 1ZYJ.pdb, stability and activity data from this work.

Thermal Stability of p38α DFG Mutants. The thermal stability of each p38α variant protein was studied by fluorescence spectroscopy. Wild-type p38α protein and the five DFG mutants were exposed to a temperature gradient from 20 °C to 80 °C, and intrinsic fluorescence was monitored continuously as described in Materials and Methods. At low temperature, the p38α proteins exist in a compact folded state. As the temperature increases, the p38α proteins unfold in a cooperative manner giving rise to the fluorescence transition, which results from a change in the environment of naturally occurring fluorophores, predominantly tryptophan side chains, in p38α. Melting temperature (T_m) is defined as the midpoint of the fluorescence transition, the temperature at which half of the protein is unfolded. Typical raw and processed thermal denaturation curves for the wild-type p38α protein and DFG mutants are shown in Figure 2. Wild-type p38α protein is relatively stable to thermal denaturation at pH 7.5; the protein begins to unfold near 49 °C and is completely unfolded at 53 °C with an estimated T_m of 50.7 °C. The DFG mutant p38α proteins exhibited a range of thermal stabilities including those more stable than wild-type p38α (p38α-D168G T_m = 54.5 °C; p38α-F169A T_m = 52.0 °C) and those less stable then wild-type p38α (p38α-F169R T_m = 46.0 °C; p38α-F169G T_m = 47.5 °C). The most conservative mutant, p38α-F169Y (T_m = 50.6 °C), showed a thermal denaturation profile closest to that of wild-type p38α. In repeated experiments the thermal denaturation curve of p38α-F169G appears to be biphasic with a major transition at 47.0 °C, and minor transition at 49.7 °C. For the remainder of this discussion a single composite T_m of 47.5 °C is used for p38α-F169G based on fitting of all of the data points as a single curve, since the apparent biphasic melting behavior is not clearly understood and does not alter the conclusions of this study.

X-ray Crystal Structures. Each DFG mutant p38α protein was crystallized as previously described, and its X-ray crystal structure was determined by molecular replacement (*16*, *23*). Crystallographic data collection and refinement statistics are given in the Supporting Information. The crystal form of p38α kinase obtained for these studies is identical to a previously reported crystal form (*24*), and the wild-type

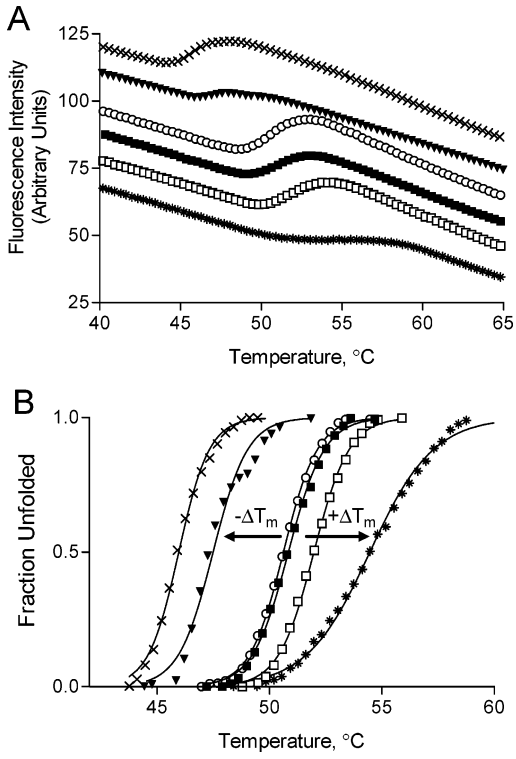

FIGURE 2: Thermal denaturation of wild-type p38α and DFG mutants assessed by fluorescence spectroscopy. Samples containing 1.8 μM protein in 25 mM Tris, pH 7.5, 100 mM sodium chloride, 10 mM $MgCl_2$, 5% glycerol, and 10 mM DTT buffer were subjected to a temperature gradient from 20 °C to 80 °C at a rate of 1 °C/min. Apparent midpoint melting temperature T_m was defined as a fluorescence transition midpoint and was extrapolated using Boltzmann sigmoidal equation as described in Materials and Methods. (A) Intrinsic fluorescence traces of wt p38α (■), p38α-F169A (□), p38α-F169Y (○), p38α-F169G (▼), p38α-F169R (×) and p38α-D168G (∗) mutants measured at an absorption maximum of 280 nm and an emission maximum of 340 nm. (B) Normalized thermal unfolding curves. Fluorescence intensity data were corrected for the baselines for the folded and unfolded protein forms and normalized to calculate the fraction of folded protein (see Materials and Methods for details). The decreased melting temperature of p38α-F169G and p38α-F169R (observed as a shift of the protein thermal melting curves to the left, $-\Delta T_m$) is an indication of structural destabilization of these mutants. The increased melting temperature of p38α-F169A and p38α-D168G (observed as a shift of the protein thermal melting curves to the right, $+\Delta T_m$) indicates that these variants are more stable than the wild-type p38α protein. The F169Y mutation did not affect the thermal stability of the p38α protein.

structure used for comparison is a previously published structure from this laboratory (1ZYJ.pdb) which contains an ATP site inhibitor that does not interact with the DFG motif and does alter the DFG conformation from that of apo-p38α (*23*). The protein is in the inactive, unphosphorylated state. Most of the activation loop (residues 173−183) and a portion of the "glycine-rich" or "P" loop (residues 31−36) (*25*) are usually not visible in the electron density maps, and these regions are presumably disordered. Secondary electron densities were observed for the DFG loops of three of the mutants, p38α-F169R, p38α-F169Y, and p38α-D168G (Table 1). In such cases, the crystallographic model that was built describes the interpretable, dominant regions of the electron density maps.

Three distinct DFG conformations were observed among the wild-type, 1KV1, 2EWA, and mutant p38α forms

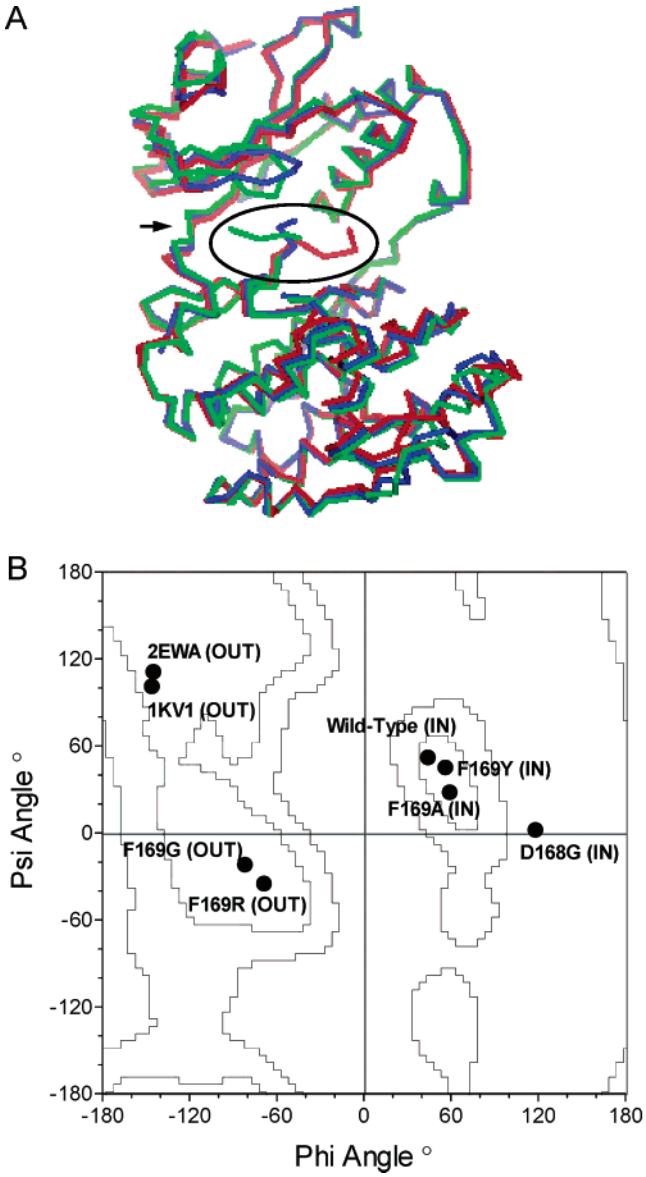

FIGURE 3: Comparison of three different DFG motif conformations. Panel A shows a superimposition of Cα traces from structures depicting the following conformations: DFG-IN as observed in PDB structure 1ZYJ.pdb (red trace); β-DFG-OUT as observed in PDB structures 1KV1.pdb (blue trace) and 2EWA.pdb; and α-DFG-OUT as observed for unliganded p38α-F169G (green trace) and p38α-F169R. Panel B shows a Ramachandran plot of φ and ψ angles for Asp168 (or Gly168 in p38α-D168G) in the different p38α DFG conformations. The inner contour encloses preferred conformational regions, and the outer contour encloses allowed regions for all amino acids (except proline and glycine) as defined by Lovell et al. (*28*). All Asp168 conformations fall within preferred regions for aspartic acid, and Gly168 of p38α-D168G falls within a preferred region for glycine.

(Figure 3A). In the absence of a bound inhibitor, wild-type p38α was found exclusively in the DFG-IN conformation, while p38α-F169G was found exclusively in a DFG-OUT conformation and p38α-F169R was found predominantly in the same DFG-OUT conformation. The novel DFG-OUT conformation observed for the unliganded p38α mutants studied here is structurally distinct from the DFG-OUT conformation reported for the inhibitor bound p38α structures 1KV1 and 2EWA. Most of the local conformational change in the DFG-IN to DFG-OUT transition of p38α is centered on Asp168, and the φ and ψ torsion angles of Asp168 clearly

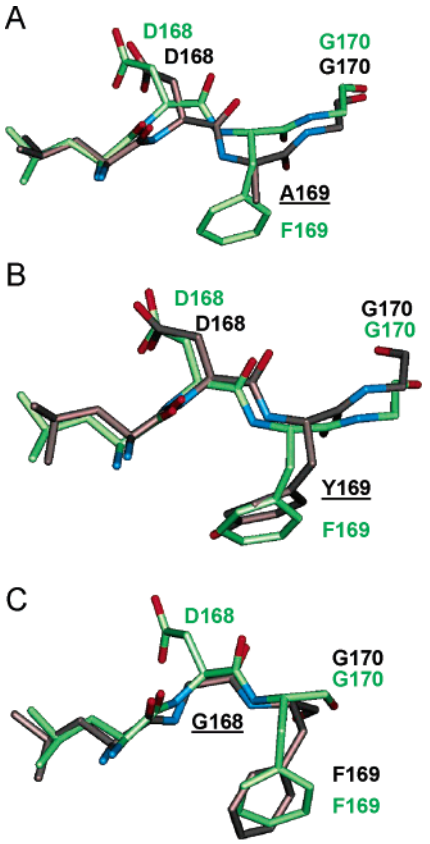

FIGURE 4: DFG-IN conformations observed for p38α-F169A (panel A), p38α-F169Y (panel B), and p38α-D168G (panel C). In each case, the mutant trace is shown with gray carbons, and the wild-type trace (from PDB entry 1ZYJ.pdb, a previously published structure in the same crystal form) is shown with green carbons for comparison. Key residues are noted.

segregate the observed DFG conformations into different structural regions (Figure 3B).

Despite the loss of almost all side chain surface area (~200 Å^2) in p38α-F169A, the observed conformation of the DAG motif is similar to the DFG-IN conformation of wild-type p38α (Figure 4A). To compensate for the loss of side chain surface area, the DAG motif in p38α-F169A undergoes a change that can best be described as a "collapse" which results in the Ala side chain partially filling the cavity that is normally occupied by the Phe169 side chain in wild-type p38α. Specifically, the alanine Cβ of F169A occupies approximately same position as the Phe169 Cγ of wild-type p38α. In p38α-F169A, there are significant van der Waals contacts between the Ala side chain and the surface of the Phe169 pocket as well as a hydrogen bond between main chain atoms which contribute to the stability of the observed DAG-IN conformation. Although the conformation of the DAG motif in p38α-F169A is similar to the DFG-IN conformation observed in wild-type p38α, there are small but notable changes in the φ and ψ angles of Asp168 ($\Delta\varphi = +15°$ and $\Delta\psi = -24°$) related to significant shifts (~1 Å) in the position of the Asp168 side chain atoms.

The dominant conformation of the DYG motif in p38α-F169Y is similar to the DFG-IN conformation of wild-type p38α (Figure 4B). The larger tyrosine side chain in p38α-F169Y is accommodated in the Phe169 pocket by small changes in the Asp168 φ and ψ angles ($\Delta\varphi = +12°$ and $\Delta\psi = -7°$), resulting in small shifts (~0.5 Å) in the position of the Asp168 side chain atoms.

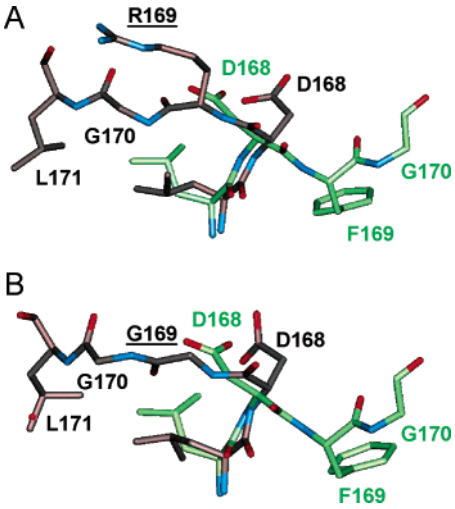

FIGURE 5: DFG-OUT conformations observed for p38α-F169R (panel A) and p38α-F169G (panel B). In each case, the mutant trace is shown with gray carbons and the wild-type trace (from 1ZYJ.pdb, a previously published structure in the same crystal form) is shown with green carbons for comparison. Key residues are noted.

The $2F_o - F_c$ electron density map for p38α-D168G is associated with fragmented electron density which suggests the presence of disorder in the region of the GFG sequence. However, the electron density map was sufficient to produce a model of the GFG-IN conformation of p38α-D168G, which was found to be similar to that of wild-type p38α (Figure 4C). In the p38α-D168G GFG-IN state there are large changes in the φ and ψ angles of Gly168 ($\Delta\varphi = +74°$ and $\Delta\psi = -50°$) with respect to the DFG-IN state of Asp168 in the wild-type DFG motif. The result is that the Phe169 side chain lies somewhat deeper in the pocket and the GFG backbone makes more van der Waals contacts than in wild-type p38α.

The dominant conformation of the DRG motif in p38α-F169R is a DRG-OUT conformation that is distinct from the DFG-IN conformation of wild-type p38α (Figure 5A), characterized by large differences in the Asp168 φ and ψ torsion angles compared to the wild-type DFG-IN conformation ($\Delta\varphi = -113°$ and $\Delta\psi = -87°$). This DRG-OUT conformation is also markedly different from the inhibitor-bound DFG-OUT conformation seen in PDB entry 1KV1, as characterized by large differences in the φ and ψ torsion angles of Asp168 ($\Delta\varphi = +77°$ and $\Delta\psi = -136°$), and from the related inhibitor-bound DFG-OUT structure 2EWA (9, *15*). In the p38α-F169R DRG-OUT conformation, the side chain of Arg169 is largely disordered beyond the beta carbon and the side chain of Leu171 is well-resolved and lies in the vicinity of the hinge region more than 10 Å away from its original position, where it is stabilized by hydrophobic interactions with residues Leu167 and Met109.

p38α-F169G adopts a DGG-OUT conformation almost identical to p38α-F169R (Figure 5B). No significant electron density is observed that would indicate the presence of a DGG-IN conformation. Like the p38α-F169R DRG-OUT conformation, the p38α-F169G DGG-OUT conformation is characterized by large differences in the Asp168 φ and ψ torsion angles compared to the wild-type DFG-IN conformation ($\Delta\varphi = -126°$ and $\Delta\psi = -74°$) and compared to the

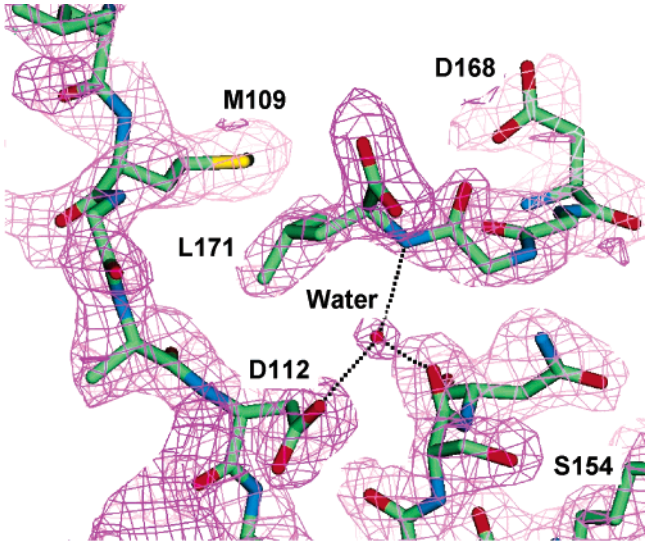

FIGURE 6: Water stabilizes the DFG-OUT conformation of p38α-F169G. The electron density is shown in mauve wireframe, and the structural model is shown in standard atom colors. Leu171 is observed to occupy the pocket near Met109 in the region of the ATP binding site. The dotted lines represent hydrogen bonds that may be contributing to the stability of this conformation.

inhibitor-bound DFG-OUT conformation seen in PDB entry 1KV1 ($\Delta\varphi = +64°$ and $\Delta\psi = -123°$) (*9*). Similar to the p38α-F169R DRG-OUT conformation, the side chain of residue Leu171 in the p38α-F169G DGG-OUT conformation lies in the vicinity of the hinge region more than 10 Å away from its original position, where it is stabilized by hydrophobic interactions with residues Leu167 and Met109. In p38α-F169G (Figure 6) a water molecule is involved in stabilizing the DGG-OUT conformation by bridging the side chain caboxylate of Asp112, the backbone carbonyl of Ser154, and the main chain NH of Leu171. It is possible that this tricoordinated water molecule provides enough additional stability to account for the fact that only the DGG-OUT conformation is observed for p38α-F169G. Additionally, the glycine-rich loop (P-loop) and Tyr35 are also partially resolved in the electron density map, indicating that the p38α-F169G DGG-OUT conformation plays a role in stabilizing this highly dynamic loop that is usually disordered in p38α crystal structures.

DISCUSSION

The DFG (Asp-Phe-Gly) motif located at the beginning of the activation loop of p38α is highly conserved across the protein kinase superfamily and is a structurally dynamic feature of many protein kinases including p38 (*5*, *26*, *15*). In p38α, the DFG loop undergoes structural reorganization upon binding of diarylurea inhibitors, resulting in a large (~10 Å) shift of the Phe169 residue side chain from a buried position (DFG-IN) to a relatively solvent exposed position (DFG-OUT) (*9*). Inhibitors that bind in this manner are often called allosteric inhibitors. Much attention has been focused on the discovery of such allosteric inhibitors for p38α and other protein kinases (*13*, *25*), and the mechanism by which allosteric inhibitors are able to bind to p38α and stabilize the DFG-OUT conformation is beginning to emerge. Frembgen-Kesner et al. recently reported that the DFG-OUT conformation could be observed during high-temperature molecular dynamics simulations of p38α and that diarylurea inhibitors such as BIRB-796 could bind, although infrequently, to the DFG-IN conformation. They also reported observing two new DFG conformations, a pseudo-DFG-IN and a pseudo-DFG-OUT conformation (*14*). Vogtherr et al. recently provided NMR evidence supporting the existence of a dynamic equilibrium between DFG-IN and DFG-OUT conformations of p38α in the absence of an inhibitor and a cocrystal structure showing SB-203580 bound to the ATP-binding site of p38α in both DFG-IN or DFG-OUT conformations in approximately equal proportions (*15*).

To examine the role of Phe169 in the structure and function of the DFG loop in p38α MAP kinase, we have constructed five p38α DFG mutant proteins and analyzed them for activation by MKK6, protein kinase activity, and thermal stability. Crystal structures of the five p38α DFG mutants were also solved. The secondary structure preceding the DFG motif in wild-type p38α is a beta strand extending from Cys162 to Leu167. The φ and ψ angles of the residues within this beta strand remain largely constant between wild-type, 1KV1, 2EWA, and all of the DFG mutants studied here, although the φ and ψ angles for Leu167 in 1KV1 segregate somewhat from those of the other structures within the allowed beta region. It is interesting to note that Phe169 adopts a beta-like conformation in all of the studied p38α forms, however it falls outside of the allowed-but-disfavored beta region in the 1KV1 structure indicating that it is in an energetically disfavored state compared to the other conformations. It is likely that the higher energy state of Phe169 in 1KV1 is compensated by the inhibitor binding energy, and this suggests that the exact DFG-OUT state observed in 1KV1 is unlikely to occur in the absence of inhibitor.

The structures of p38α-F169R and p38α-F169G adopt a DFG-OUT conformation in the absence of inhibitor, and this conformation is structurally distinct from the previously described inhibitor-stabilized DFG-OUT conformation of p38α (*9*, *15*) (Figure 3A). For the p38α DFG mutants studied here, the diarylurea-bound p38α structures 1KV1 and 1KV2, and the recently described pyrazole inhibitor-bound structure 2EWA, the DFG-IN to DFG-OUT transition is centered on Asp168, and the φ and ψ angles for Asp168 in the corresponding DFG-IN and DFG-OUT forms fall into three different structural regions (Figure 3B) which can be used to classify the DFG conformations (*27*, *28*). In the DFG-IN conformation of wild-type p38α, p38α-F169A, p38α-F169Y, and p38α-D168G, Asp168 adopts a left-handed alpha-helix-like conformation (α_L), whereas Asp168 in the DFG-OUT conformation observed in PDB structures 1KV1 and 2EWA continues the beta sheet conformation (β), and the DFG-OUT conformation of Asp168 in p38α-F169G and p38α-F169R adopts a right-handed alpha-helix-like conformation (α_R). In order to clearly distinguish the newly observed DFG-OUT conformation in p38α-F169G and p38α-F169R, it can be denoted as α-DFG-OUT to reflect the right-handed alpha-helix-like conformation of Asp168. Accordingly, the previously observed DFG-OUT conformation of 1KV1 and 2EWA can be denoted as β-DFG-OUT to reflect the beta-sheet-like conformation of Asp168. Although φ and ψ angles are not given for the pseudo-DFG-OUT computationally predicted by Frembgen-Kesner (*14*), it appears to be distinct from the α-DFG-OUT conformation observed here for p38α-F169R and p38α-F169G. In the pseudo-DFG-OUT conformation reported by Frembgen-Kesner, Leu171 occupies the

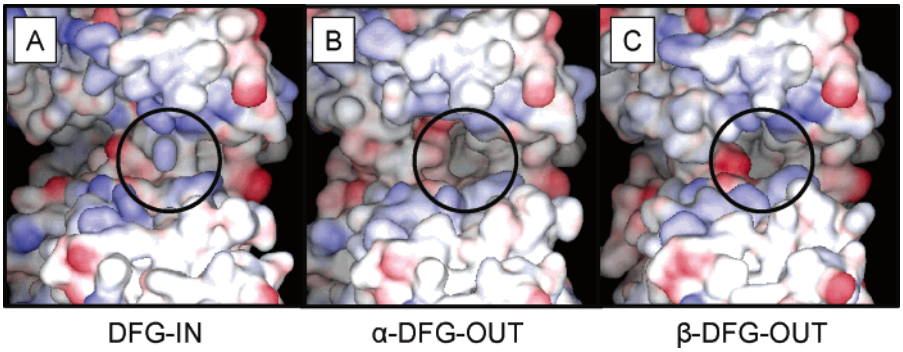

FIGURE 7: Putative allosteric inhibitor entry pocket in p38α-F169G. Solvent exposed surfaces in the active site cleft of p38α reveal a potential point of entry for allosteric inhibitors (indicated by circle). Panel A: DFG-IN, wild-type p38α bound to an ATP site inhibitor (inhibitor not shown) from PDB entry 1ZYJ. Panel B: α-DFG-OUT, p38α-F169G. Panel C: *β*-DFG-OUT, wild-type p38α bound to an allosteric site inhibitor (inhibitor not shown) from PDB entry 1KV1.

pocket vacated by Phe169, whereas the Phe169 pocket is open and Leu171 resides near Met109 in the α-DFG-OUT conformation of p38α-F169G and p38α-F169R.

Based on the thermal stabilities and structures of wild-type p38α and the p38α DFG mutants, the α-DFG-OUT state is energetically less favorable than the DFG-IN state but appears to be an allowed state that may exist at physiologically relevant temperatures. Thus, the α-DFG-OUT state could provide a transient route of entry for allosteric inhibitors that bind to the *β*-DFG-OUT state (Figure 7). In both the α-DFG-OUT state of p38α-F169G and p38α-F169R and the *β*-DFG-OUT state of 1KV1 and 2EWA, the ATP site is partially occluded by the DFG loop. In the wild-type p38α DFG-IN state, the Phe169 pocket is occluded while the ATP site is open (Figure 7A). In contrast, the Phe169 pocket is open in the α-DFG-OUT state of p38α-F169G (Figure 7B) and p38α-F169R in much the same way it is open in the *β*-DFG-OUT state observed in the inhibitor-bound 1KV1 structure (*9*) (Figure 7C). However, in 1KV1 and 2EWA the *β*-DFG-OUT conformation is driven by inhibitor binding, while in p38α-F169G and p38α-F169R the α-DFG-OUT conformation is driven solely by protein dynamics.

No differences were observed in the ability of MKK6 to phosphorylate the p38 variants *in vitro*, regardless of a preference for the DFG-IN or DFG-OUT state (Table 1). This is of interest because DFG-OUT-inducing (allosteric) inhibitors of p38α such as BIRB-796 have been shown to bind to unphosphorylated p38α and inhibit its phosphorylation (activation) by MKK6 in purified preparations and in cells (*29*). It has been postulated that disorder in the activation loop induced by the allosteric inhibitors makes the p38α activation loop a poor substrate for MKK6 (*22*). Recently, the naturally occurring DFD motif in Mnk2 kinase was shown to exist in a DFD-OUT conformation in the absence of a bound ligand (*30*). The preference of Mnk2 for the DFD-OUT conformation does not preclude binding of ATP, suggesting that ATP can induce the DFD-IN conformation in Mnk2. Thus, it is possible that in the absence of inhibitor MKK6 can force the DFG-IN conformation in p38α even in the case of p38α-F169G and p38α-F169R. Alternatively, the α-DFG-OUT conformation observed for p38α-F169G and p38α-F169R could still be compatible with phosphorylation of Thr180 and Tyr182 by MKK6, while the *β*-DFG-OUT conformation is not.

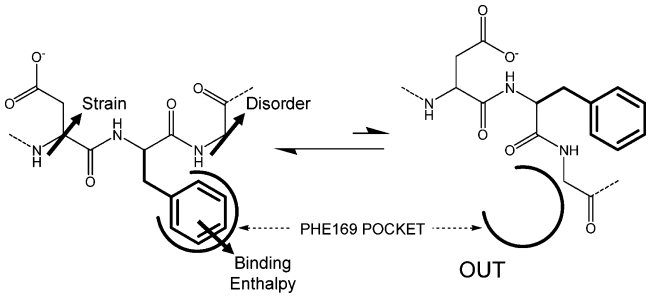

FIGURE 8: Cartoon model of forces driving DFG loop dynamics in p38α. Arrows indicate strain in Asp168 and disorder in Gly170 which oppose the binding enthalpy of occupancy of the Phe169 pocket. Strain and disorder facilitate the DFG loop dynamic transition, while the binding enthalpy stabilizes the DFG-IN conformation required for p38α catalytic activity.

Of the p38α variants studied here, only p38α-F169Y possesses detectable catalytic activity for phosphorylation of GST-ATF2 compared to wild-type p38α (Table 1). Since Phe169 is not known to participate directly in p38α catalysis, it is likely that the observed loss of activity in the Phe169 mutants is related to an effect on local structure. Changes in the positioning of Asp168 (Table 1) observed in the unactivated p38α Phe169 mutants studied here suggest that the loss of kinase activity may result from aberrant positioning of Asp168 in the activated form. The conformation of the DFG motif in the unactivated wild-type and DFG-IN mutant p38α structures described here appears to be substantially similar to the proposed activated conformation of p38α. This finding is supported by comparison to the published activated structure of the closely related MAP kinase p38*γ* (1CM8.pdb) (*31*) and to changes expected to occur upon protein kinase activation according to the recently reported activation "spine" concept (*32*). Even in unactivated p38α, the α-C-helix is rotated inward, the K53-E71 ion pair is present, and H148 is in hydrophobic contact with F169, A169, or Y169 of the p38α variants studied here. The hydrophobic spine of unactivated p38-alpha is also substantially similar to the putative activated state of p38α. For p38α, the major effect of activation according to the activation "spine" model and studies conducted on the related protein kinase ERK2 (*33*) appears to be realignment of Arg149 to make polar contact with the DFG motif and orient the side chain of Asp168. While this likely has an effect of further stabilizing the DFG-IN conformation of p38α, it does not appear to be a prime determinant of the local DFG conformation even in the unactivated state of p38α. Thus,

the DFG-IN positioning of Asp168 in unactivated p38α is likely to be representative of its position in activated p38α, and the substantial loss of activity observed for p38α-F169Y and p38α-F169A suggests that p38α catalytic activity is extremely sensitive to positioning of Asp168 as observed in ERK2 (*33*).

DFG mutants p38α-F169A and p38α-D168G were significantly more thermostable than wild-type p38α (Table 1). The increased stability of these mutants clearly indicates that the DFG motif is not optimal for p38α structural stability. This is consistent with prior observations for T4 lysozyme and supports the general assertion that catalytic residues in proteins are optimized for function rather than structural stability (*34*).

Based on the structural and functional data from wild-type p38α and the five DFG mutants described here, a hypothetical model of p38α DFG loop structural dynamics is proposed (Figure 8). In this model, conformational strain expressed in the Asp168-Phe169 backbone and disorder expressed in the activation loop beginning from Gly170 promote the DFG-OUT transition. Conversely, surface contacts in the Phe169 pocket provide enough binding enthalpy to promote the DFG-IN conformation even in cases where the Phe169 side chain is substantially extended (p38α-F169Y, p38α-F169R) or minimized (p38α-F169A).

Taken together, these results suggest that Phe169 in p38α is optimized for functional activity and structural dynamics, rather than for structural stability. Conformational plasticity of the p38α activation loop, and particularly the DFG motif, may exist in the natural distribution of dynamic states of p38α in the absence of inhibitor binding, and the novel α-DFG-OUT conformation observed for p38α-F169R and p38α-F169G may serve as an intermediate state that allows binding of allosteric inhibitors to wild-type p38α. A natural functional role is yet to be ascribed to this conformational switch in p38α but may include a mechanism of conformational autoinhibition (*35*, *36*) or a mechanism for partnering with other proteins (*37*) as observed for other protein kinases.

ACKNOWLEDGMENT

The authors thank William Moore, Jeff Wiseman, and Dagmar Ringe for their helpful review of the manuscript. The authors are grateful to Xiaomei Chai and Ken Williams for excellent technical assistance. Ramachandran plot contours were obtained from the kinemage website of the Richardson lab at Duke University: http://kinemage.biochem.duke.edu.

SUPPORTING INFORMATION AVAILABLE

Crystallographic data collection and refinement statistics are given in Table 2 and electron densities associated with the DFG motif models are given in Figures 9 and 10 for p38α mutant forms p38α-D168G, p38α-F169A, p38α-F169Y, p38α-F169G, and p38α-F169R. This material is available free of charge via the Internet at http://pubs.acs.org.

REFERENCES

1. Lee, J. C., Laydon, J. T., McDonnell, P. C., Gallagher, T. F., Kumar, S., Green, D., McNulty, D., Blumenthal, M. J., Heys, J. R., Landvatter, S. W., Strickler, J. E., McLaughlin, M. M., Siemens, I. R., Fisher, S. M., Livi, G. P., White, J. R., Adams, J. L., and Young, P. R. (1994) A protein kinase involved in the regulation of inflammatory cytokine biosynthesis, *Nature 372*, 739−746.
2. Han, J., Lee, J. D., Bibbs, L., and Ulevitch, R. J. (1994) A MAP kinase targeted by endotoxin and hyperosmolarity in mammalian cells, *Science 265*, 808−811.
3. Herlaar, E., and Brown, Z. (1999) p38α MAPK signaling cascades in inflammatory disease, *Mol. Med. Today 5*, 439−447.
4. Lee, J. C., Kumar, S., Griswold, D. E., Underwood, D. C., Votta, B. J., and Adams, J. L. (2000) Inhibition of p38α MAP kinase as a therapeutic strategy, *Immunopharmacology 47*, 185−201.
5. Johnson, L. N., Noble, M. E., and Owen, D. J. (1996) Active and inactive protein kinases: structural basis for regulation, *Cell 85*, 149−158.
6. Nolen, B., Taylor, S., and Ghosh, G. (2004) Regulation of protein kinases: controlling activity through activation segment conformation, *Mol. Cell 15*, 661−675.
7. Kannan, N., and Neuwald, A. F. (2005) Did protein kinase regulatory mechanisms evolve through elaboration of a simple structural component?, *J. Mol. Biol. 351*, 956−972.
8. Levinson, N. M., Kuchment, O., Shen, K., Young, M. A., Koldobskiy, M., Karplus, M., Cole, P. A., and Kuriyan, J. (2006) A Src-like inactive conformation in the Abl tyrosine kinase domain, *PLoS Biol. 4*, 753−767.
9. Pargellis, C., Tong, L., Churchill, L., Cirillo, P. F., Gilmore, T., Graham, A. G., Grob, P. M., Hickey, E. R., Moss, N., Pav, S., and Regan, J. (2002) Inhibition of p38 MAP kinase by utilizing a novel allosteric binding site, *Nat. Struct. Biol. 9*, 268−272.
10. Regan, J., Breitfelder, S., Cirillo, P., Gilmore, T., Graham, A. G., Hickey, E., Klaus, B., Madwed, J., Moriak, M., Moss, N., Pargellis, C., Pav, S., Proto, A., Swinamer, A., Tong, L., and Torcellini, C. (2002) Pyrazole urea-based inhibitors of p38 MAP kinase: from lead compound to clinical candidate, *J. Med. Chem. 45*, 2994−3008.
11. Mol, C. D., Fabbro, D., and Hosfield, D. J. (2004) Structural insights into the conformational selectivity of STI-571 and related kinase inhibitors, *Curr. Opin. Drug Discovery Dev. 7*, 639−648.
12. Knight, Z. A., and Shokat, K. M. (2005) Features of selective kinase inhibitors, *Chem. Biol. 12*, 621−637.
13. Liu, Y., and Gray, N. S. (2006) Rational design of inhibitors that bind to inactive kinase conformations, *Nat. Chem. Biol. 2*, 358−364.
14. Frembgen-Kesner, T., and Elcock, A. H. (2006) Computational sampling of a cryptic drug binding site in a protein receptor: explicit solvent molecular dynamics and inhibitor docking to p38 MAP kinase, *J. Mol. Biol. 359*, 202−214.
15. Vogtherr, M., Saxena, K., Hoelder, S., Grimme, S., Betz, M., Schieborr, U., Pescatore, B., Robin, M., Delarbre, L., Langer, T., Wendt, K. U., and Schwalbe, H. (2006) NMR characterization of kinase p38 dynamics in free and ligand-bound forms, *Angew. Chem., Int. Ed. 45*, 993−997.
16. Bukhtiyarova, M., Northrop, K., Chai, X., Casper, D., Karpusas, M., and Springman, E. (2004) Improved expression, purification, and crystallization of p38alpha MAP kinase, *Protein Expression Purif. 37*, 154−161.
17. Kroe, R. R., Regan, J., Proto, A., Peet, G. W., Roy, T., Landro, L. D., Fuschetto, N. G., Pargellis, C. A., and Ingraham, R. H. (2003) Thermal denaturation: a method to rank slow binding, high-affinity P38alpha MAP kinase inhibitors, *J. Med. Chem. 46*, 4669−4675.
18. Matulis, D., Kranz, J. K., Salemme, F. R., and Todd, M. J. (2005) Thermodynamic stability of carbonic anhydrase: measurements of binding affinity and stoichiometry using ThermoFluor, *Biochemistry 44*, 5258−5266.
19. Otwinowski, Z., and Minor, W. (1997) Processing of X-ray diffraction data collected in oscillation mode, *Macromol. Crystallogr. A 276*, 307−326.
20. Brunger, A. T., Adams, P. D., Clore, G. M., DeLano, W. L., Gros, P., Grosse-Kunstleve, R. W., Jiang, J. S., Kuszewski, J., Nilges, M., Pannu, N. S., Read, R. J., Rice, L. M., Simonson, T., and Warren, G. L. (1998) Crystallography & NMR system: a new software suite for macromolecular structure determination, *Acta Crystallogr. D. Biol. Crystallogr. 54*, 905.
21. Taylor, S. S., and Radzio-Andzelm, E. (1994) Three protein kinase structures define a common motif, *Structure 2*, 345−355.
22. Sullivan, J. E., Holdgate, G. A., Campbell, D., Timms, D., Gerhardt, S., Breed, J., Breeze, A. L., Bermingham, A., Pauptit, R. A., Norman, R. A., Embrey, K. J., Read, J., VanScyoc, W. S., and Ward, W. H. J. (2005) Prevention of MKK6-dependednt

activation by binding to p38α MAP kinase, *Biochemistry 44*, 16475−16490.
23. Michelotti, E. L., Moffett, K. K., Nguyen, D., Kelly, M. J., Shetty, R., Chai, X., Northrop, K., Namboodiri, V., Campbell, B., Flynn, G. A., Fujimoto, T., Hollinger, F. P., Bukhtiyarova, M., Springman, E. B., and Karpusas, M. (2005) Two classes of p38α MAP kinase inhibitors having a common diphenylether core but exhibiting divergent binding modes, *Bioorg. Med. Chem. Lett. 15*, 5274−5279.
24. Pav, S., White, D. M., Rogers, S., Crane, K. M., Cywin, C. L., Davidson, W., Hopkins, J., Brown, M. L., Pargellis, C. A., and Tong, L. (1997) Crystallization and preliminary crystallographic analysis of recombinant human p38 MAP kinase, *Protein Sci. 6*, 242−245.
25. Cherry, M., and Williams, D. H. (2004) Recent kinase and kinase inhibitor x-ray structures: mechanisms of inhibition and selectivity insights, *Curr. Med. Chem. 11*, 663−673.
26. Huse, M., and Kuriyan, J. (2002) The conformational plasticity of protein kinases, *Cell 109*, 275−282.
27. Morris, A. L., MacArthur, M. W., Hutchinson, E. G., and Thornton, J. M. (1992) Stereochemical quality of protein structure coordinates, *Proteins: Struct., Funct., Genet. 12*, 345−364.
28. Lovell, S. C., Davis, I. W., Arenall, W. B., III, de Bakker, P. I. W., Word, J. M., Prisant, M. G., Richardson, J. S., and Richardson, D. C. (2003) Structure validation by Cα geometry: φ, ψ and Cβ deviation, *Proteins: Struct., Funct., Genet. 50*, 437−450.
29. Kuma, Y., Sabio, G., Bain, J., Shapiro, N., Márquez, R., and Cuenda, A. (2005) BIRB 796 inhibits all p38 MAPK isoforms *in vitro* and in *vivo*, *J. Biol. Chem. 280*, 19472−19479.
30. Jauch, R., Jäkel, S., Netter, C., Schreiter, K., Aicher, B., Jäckle, H., and Wahl, M. C. (2005) Crystal Structure of Mnk2 kinase domain reveal an inhibitory conformation and a Zinc binding site, *Structure 13*, 1559−1568.
31. Bellon, S., Fitzgibbon, M. J., Fox, T., Hsiao, H. M., and Wilson, K. P. (1999) The structure of phosphorylated p38gamma is monomeric and reveals a conserved activation-loop conformation, *Structure 7*, 1057−1065.
32. Kornev, A. P., Haste, N. M., Taylor, S. S., and Ten Eyck, L. F. (2006) Surface comparison of active and inactive protein kinases identifies a conserved activation mechanism, *Proc. Nat. Acad. Sci. U.S.A. 103*, 17783−17788.
33. Lee, T., Hoofnagle, A. N., Resing, K. A., and Ahn, N. G. (2005) Hydrogen exchange solvent protection by an ATP analogue reveals conformational changes in ERK2 upon activation, *J. Mol. Biol. 353*, 600−612.
34. Shoichet, S. K., Baase, W. A., Kuroki, R., and Matthews, B. W. (1995) A relationship between protein stability and protein function, *Proc Natl. Acad. Sci. U.S.A. 92*, 452−456.
35. Hubbard, S. R., Mohammadi, M., and Schlessinger, J. (1998) Autoregulatory mechanisms in protein-tyrosine kinases, *J. Biol. Chem. 273*, 11987−11990.
36. Cheetham, G. M. T. (2004) Novel protein kinases and molecular mechanisms of autoinhibition, *Curr. Opin. Struct. Biol. 14*, 700−705.
37. Gay, L. M., Ng, H.-L., and Alber, T. (2006) A conserved dimer and global conformational changes in the structure of apo-PknE Ser/Thr protein kinase from *Mycobacterium tuberculosis*, *J. Mol. Biol. 360*, 409−420.

BI0622221